Rim nucleation and step-train orientation effects in SOI(111) dewetting

Stefano Curiotto, Pierre Müller, Fabien Cheynis, Igor Ozerov, Frédéric Leroy

Surfaces and Interfaces 45 (2024) 103912

Contents lists available at ScienceDirect

Surfaces and Interfaces

journal homepage: www.sciencedirect.com/journal/surfaces-and-interfaces

Rim nucleation and step-train orientation effects in SOI(111) dewetting

Stefano Curiotto *, Pierre Müller, Fabien Cheynis, Igor Ozerov, Frédéric Leroy

Aix Marseille University, CNRS, CINAM, Marseille, France

ARTICLE INFO

Keywords:
Kinetic Monte Carlo methods
Cluster diffusion
Finite-size effects
Electromigration

ABSTRACT

We demonstrate that the step-train orientation of a vicinal surface plays an important role in solid-state dewetting. Focusing on SOI(111), we observe the formation of hexagonal voids in the silicon film due to dewetting. These voids are surrounded by an asymmetric rim, which is wider on the higher-terrace side compared to the lower-terrace side. Our findings also reveal a layer-by-layer growth of the rim around the dewetting voids during the early stages, before the formation of branched structures. Dewetting fingers develop faster and are thinner in the step-down direction compared to the step-up direction. Kinetic Monte Carlo (KMC) simulations confirm our experimental observations and provide insights into the atomic details underlying rim and finger formation. During the initial stages of dewetting, the nucleation of a new rim layer is not required: Atoms leaving the dewetting void are captured by the adjacent upper step, leading to the growth of the upper terrace that thus surrounds the dewetting void. The nucleation of a new rim layer only becomes necessary when the distance between the edge of the void and the upper terrace increases. The energetics involved in the dewetting kinetics of SOI(111) are consistent with those of SOI(100).

1. Introduction

Thin films deposited on a substrate are often unstable and tend to agglomerate and form isolated particles. This process, known as dewetting, occurs not only in the liquid state, but also in the solid state, at temperatures well below the melting point. Dewetting is driven by the minimization of the surface and interfacial energies. Generally, the process starts at film defects, like grain boundaries, holes, inclusions, or film edges. Then, the film morphology evolves, mediated by surface diffusion. The important morphological changes taking place during solid state dewetting can render devices inoperative. This problem is of particular concern for metal silicides and silicon on insulator (SOI) used in microelectronic devices [1,2]. Several methods to avoid or to stop dewetting have thus been explored (for a review see [3]). While dewetting limits the reliability of some devices, on the other hand, it can also be used to obtain isolated particles on a substrate. Several studies have been devoted to form organized patterns of 3D particles on a substrate by dewetting, some examples are presented in [4–11].

SOI is particularly suitable for understanding the dewetting mechanisms from a fundamental point of view because (i) as the film is a single crystal, there is no grain boundary where agglomeration could start or perturb the process and (ii) the amorphous substrate allows neglecting interfacial structure effects. In this work we focus on the effect of a parameter that is often overlooked in dewetting studies: the role of atomic steps at the surface of the thin film and in particular the step-train orientation at the surface. Atomic steps on the surface of materials are of paramount importance in materials science, for instance they affect reaction rates in catalysis, are crucial in crystal growth and nanostructure formation, and can have an effect on material wettability. We show that the step-train orientation affects both (i) the morphological anisotropy of the rim of dewetting voids, and (ii) the main propagation direction, the kinetics and the thickness of dewetting fingers. In the early dewetting stages, before the formation of branched structures, the rim around the voids grows layer by layer. Furthermore, while SOI(100) has been widely studied [4,12–17], we here investigate dewetting of SOI thin films close to the (111) orientation. From a "control" point of view, the film orientation is a parameter that can be used to obtain specific arrangements of particles by dewetting. Often thin films of materials with fcc structure adopt (111) surface orientation because growth along the [111] direction corresponds to the highest packing density of atoms [18–20]. The Si (111) surface has a 3-fold symmetry and can be considered similar to fcc materials with (111) surface orientation, therefore our results should be relevant for several other systems.

2. Experimental and modeling details

SOI(111) wafers with Si thickness of 1 ± 0.1 μm were supplied by Siegert Wafer GmbH. From a wafer, squares of 1×1 cm^2 are cut with

* Corresponding author.
E-mail addresses: stefano.curiotto@cnrs.fr (S. Curiotto), pierre.muller@univ-amu.fr (P. Müller), fabien.cheynis@univ-amu.fr (F. Cheynis), igor.ozerov@univ-amu.fr (I. Ozerov), frederic.leroy.3@univ-amu.fr (F. Leroy).

https://doi.org/10.1016/j.surfin.2024.103912
Received 19 October 2023; Received in revised form 10 January 2024; Accepted 15 January 2024
Available online 19 January 2024

a wire saw. Then, the Si (111) layer of the samples is thinned to a thickness of about 30–60 nm by reactive ion etching in SF_6 plasma. The etching rate is monitored by a laser interferometer and the final Si (111) layer thickness values are measured by a laser ellipsometer (Sentech SE400) and a contact profilometer (Bruker Dektak XT). The sample surfaces are chemically cleaned with the procedure described in [21]. In the last preparation step, a thin protective oxide layer is obtained. The *in-situ* observations are carried out in a low energy electron microscope (LEEM III, Elmitec Gmbh). The samples are introduced in Ultra High Vacuum (UHV) and degassed at about 1000 K for several hours. They are then annealed at temperatures around 1030 K to remove the protective oxide layer. The temperature is slowly increased, while observing the sample surface to detect regions where dewetting starts. The LEEM is operated in bright field mode, using electron energies below 3 eV. The images are acquired at rates of 0.1–1 Hz. In this work we have not observed surface modifications due to the long time exposure of the samples to the electron beam. In LEEM, the electrons interacting with the sample have energies lower than 10 eV, and in this work we have only used electron energies lower than 5 eV. In the LEEM community, it is usually considered that low energy electrons are scattered from the outer parts of the surface potential and that the electrons used for imaging do not affect chemical processes or surface phenomena [22]. Furthermore, the results of SOI dewetting obtained by LEEM in previous studies are consistent with the results obtained with different techniques, particularly as regards the atomic diffusion energies [14]. We thus assume that the electrons hitting the sample have a negligible effect on dewetting. The temperatures are measured with a precision of 30 K, using a disappearing-filament pyrometer, calibrated with the 7×7 to 1×1 surface phase transition occurring on Si(111) at 1103 K [23]. After the LEEM experiments, the samples are studied in air by atomic force microscopy (AFM) in tapping mode, out of the UHV, in a Park XE-100. A JEOL JSM 7900F is used for scanning electron microscopy (SEM).

Simulations are performed using a 3D kinetic Monte Carlo (KMC) model developed specifically for this work, based on a fcc lattice where the (111) plane is parallel to the substrate and to the film surface, or is slightly misoriented to address the role of the step orientation. A general introduction to the KMC method can be found in [24], and details on 3D KMC models are available in [25]. Simulations performed with our model are suited for comparisons with several metallic thin films showing fcc structure and (111) surface orientation (e.g. Au, Ni, Cu). Silicon has a diamond-like crystal structure, which is a fcc Bravais lattice with a 2-atom pattern. Since the atomic steps on the Si(111) surface are bi-layer steps, modeling by a fcc lattice is relevant.

In our model, atoms can only occupy positions of the fcc lattice. Atoms can exclusively migrate to lattice positions with neighbors. These locations include the film and the substrate surface. The simulation box has in-plane periodic boundary conditions, meaning that atoms going out from one side of the box reappear at the opposite side. Atoms jump to unoccupied neighboring lattice positions with probabilities proportional to $v_0 \exp[-(n J - E_S \delta_S)/(kT)]$, with n the number of nearest neighbors, J is the binding energy (taken as the energy unit), T is the temperature and k is the Boltzmann constant. The jump attempt frequency v_0 defines our unit time, and is assumed to be equal for all atoms. The time step between jumps is taken as the inverse of the sum of all the jump rates [24]. E_S is the film/substrate excess energy and defines the wetting properties between the substrate and the film: $E_S = \gamma_{film} + \gamma_{interface} - \gamma_{substrate}$, with γ the surface and interfacial energies. E_S is related to the film/substrate contact angle θ: as from the Young equation $\gamma_{film} \cos\theta = \gamma_{substrate} - \gamma_{interface}$, then $E_S = \gamma_{film}(1 - \cos\theta)$. In the simulations, E_S is fixed to $2.99J$ (strong dewetting tendency to speed-up simulations). δ_S is 1 for the atoms of the first film layer, i.e. at the interface with the substrate, and 0 for the other atoms. For further information on E_S and γ, see the supplementary material in [25]. In the simulations, the atomic jumps are selected according to a rejection-free Monte Carlo algorithm written in Fortran 90. At each step of the main algorithm cycle, a jump is chosen and the time advances by one time step. The new number of neighbors of the lattice positions around the starting and the arrival positions is calculated. Then the new jump rates are defined for all the atoms whose neighbors have changed, and the cycle can start again.

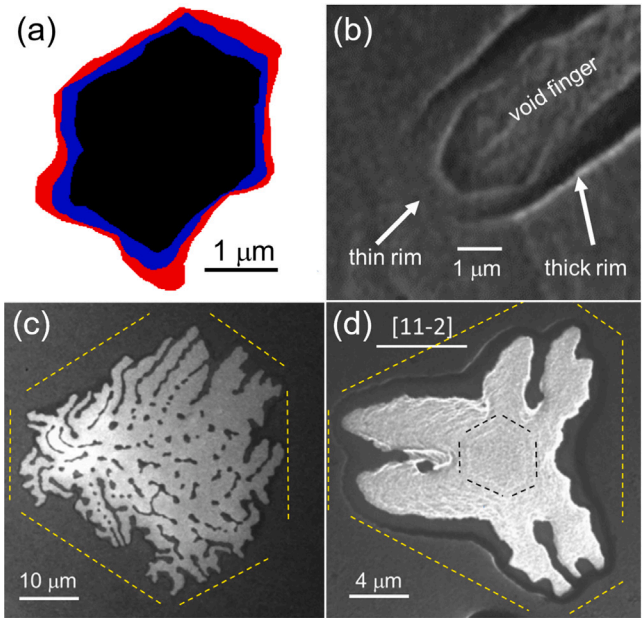

Fig. 1. (a): stroboscopic image made from three LEEM images (bright field, 5 eV electron energy, 1140 K). The blue and the red shapes are taken 493 s and 888 s after the black one. The initial void shape is hexagonal, but in later stages the corners dewet faster and from there fingers start developing. (b): void finger with a thin rim at the tip and thicker rim at the edges. (c): In advanced stages of dewetting the initial hexagonal shape of the void is only barely visible, the development of fingers in the 3-fold symmetry of the (111) SOI surface makes the total dewetted area look hexagonal with three sides longer than the other three. This is more evident in image (d) taken in another area of the sample. The initial hexagonal shape of the void can be recognized from the weak white lines due to SiO_2 etching in the reaction between Si and SiO_2 [26,27]. (For interpretation of the references to color in this figure legend, the reader is referred to the web version of this article.)

3. Void opening and dewetting in SOI(111)

As expected, we have observed by LEEM that in SOI(111) the voids that form in the initial stages of dewetting are hexagonal and not square, as in SOI(100) (see Fig. 1a) . These results are in agreement with those reported by [28,29]. Fig. 1a is a stroboscopic image of a void opening in SOI(111) at 1140 K. The void areas after 493 s and 888 s with respect to the black shape are represented in blue and red, respectively. The image shows that, during dewetting, the void area increases and the hexagonal shape is destabilized from the corners, where dewetting fingers develop. Increasing the temperature accelerates the finger formation. Silicon material accumulates in a rim around the void. When fingers develop, no rim is visible at the finger tip (see Fig. 1b). In advanced stages of dewetting, the initial hexagonal shape of the void is only barely visible (see Figs. 1c and 1d). The fingers have no fixed direction, however often they are observed to propagate in < 11-2> directions. Therefore, as shown in Fig. 1(d), the total dewetted area looks like a hexagon with three long and three short sides.

AFM observations provide further insights into the early stages of dewetting. The defect where dewetting starts is most often a protrusion (see Figs. 2a and 2b) or a hole in the SiO_2 substrate (see SEM results in Fig. 4). However we have also observed dewetting regions with no apparent starting defect, therefore coalescence of vacancies as origin of dewetting cannot be excluded [25,30]. When the dewetting region has

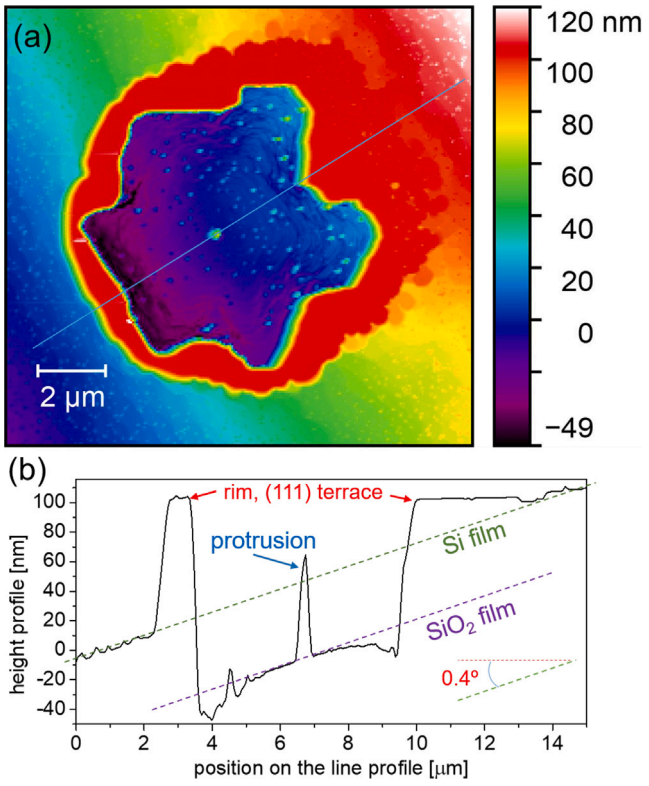

Fig. 2. (a): AFM image of a dewetting void in the first formation stages, before the development of long fingers. The red area around the void is a rim that displays a surface with no steps, i.e. a uniform atomic terrace of orientation (111). (b): Height profile taken along the blue line in (a). The unperturbed Si film and the SiO_2 substrate are roughly parallel and form an angle of 0.4° with the rim surface. The angle is measured between the line of the Si film and the horizontal given by the (111) surface of the top of the rim. Close to the rim, the SiO_2 substrate has been etched in the $Si+SiO_2=2SiO$ (gas) reaction. (For interpretation of the references to color in this figure legend, the reader is referred to the web version of this article.)

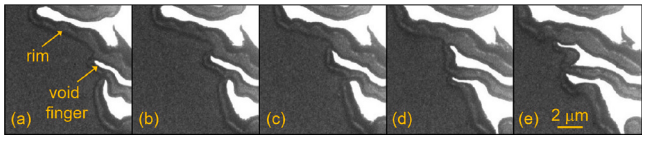

Fig. 3. (a)–(e): sequence of LEEM images (2 eV electron energy, 1130 K) showing that dewetting fingers preferentially develop along the rim of already formed fingers.

not yet formed fingers, the top of the rim where Si accumulates is a flat (111) terrace. This is evidenced in Fig. 2a, where a circular region surrounding the dewetted zone shows no height variations (uniform color and no steps), and in the height profile of Fig. 2b, taken along the blue line of Fig. 2a. Notice that the vicinal Si surface formed by successive flat terraces alternating with monoatomic steps is globally parallel to the SiO_2 substrate but forms an angle of 0.4 degrees with the (111) plane (the top of the rim). The rim is asymmetric: narrow and high with respect to the nearby film terraces on the step-down side (bottom left in Fig. 2a), and wide and low in the step-up direction (top right in Fig. 2a). This rim morphology is also observed by SEM (see later).

The initial hexagonal shape is unstable with respect to void finger formation. The dewetting fingers advance much faster than the hexagonal void edges. They do not always follow crystallographic directions, however, especially at low temperatures, they are preferentially oriented along < 211> directions. As shown in the LEEM image sequence of Fig. 3, fingers develop close to the rim of already dewetted area, as the atomic steps available in already formed rims act as sinks

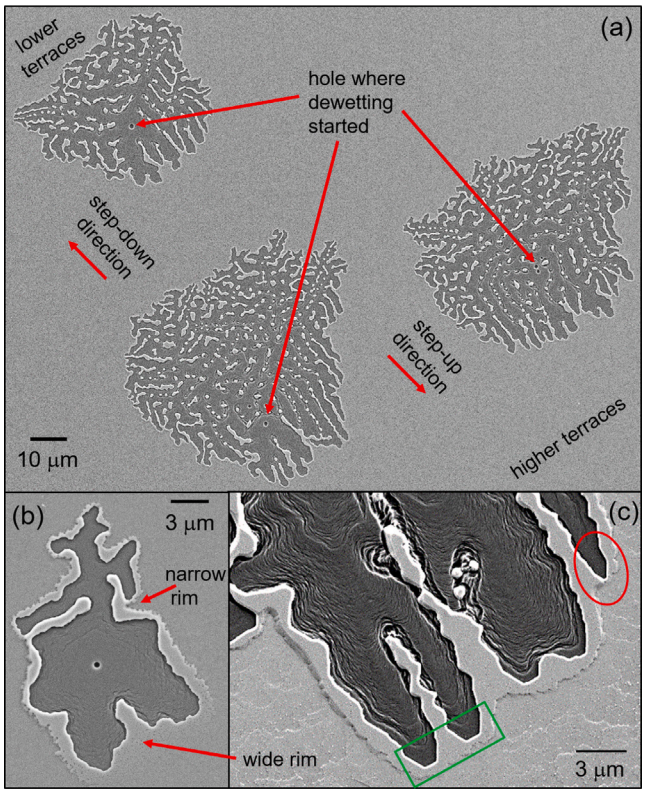

Fig. 4. (a): SEM image showing three dewetting regions. They have all started from a void, have developed large and short fingers in the step-up directions, and thin, branched fingers in the step-down direction. (b): SEM image showing that the rim around a dewetting void is wider on the step-up side than on the step-down side, where branched fingers develop. (c): highlight of the wavy shape of dewetting fingers. Notice that fingers can have sharp tips with no rim (top right), or can be faceted and display a rim. The lines inside the void fingers are due to the reaction between Si and SiO_2 to form SiO.

of adatoms, while far from rims, atoms removed from the Si/SiO_2 interface would have more chances to diffuse back into the void finger (which would thus develop slowly). The SEM image of Fig. 4a shows that the hole where dewetting (presumably) started is closer to the higher terraces than to the lower terraces. Furthermore the void fingers are thinner and develop more in the step-down direction than the fingers that form in the step-up direction (see Fig. 4b, where the wider rim on the higher-terrace side is also visible). Therefore the step-train orientation of the vicinal surface strongly affects dewetting. Fig. 4c shows that dewetting fingers are often wavy. The void finger on the top-right of the image (red ellipse) has a sharp tip with no rim, while other finger tips are faceted and have a rim (green rectangle). As observed by LEEM and KMC, void fingers with a sharp tip advance faster than fingers with a faceted tip and an extended rim. Etch lines due to the reaction between Si and SiO_2 to form volatile SiO [26] are also visible within the voids.

By LEEM, we have been able to study the dewetting mechanism in the initial stages of void opening, when well-branched fingers have not yet developed. Fig. 5 shows some snapshots of the movie available as supplementary material. The dewetting void of Fig. 5a is surrounded by a rim. The nucleus of a new rim layer has already formed and is growing in Fig. 5b (see the arrow). The rim layer extends around the dewetting void in Fig. 5c. Then the rim widens (Fig. 5d). This observation proves that the terraces around the void visible in Fig. 5a are lower than the rim, otherwise the rim would form by extension of the terraces from the exterior to the interior of the void, without nucleation of a new rim layer. After a certain time the process described above is repeated, and the height of the rim increases layer by layer.

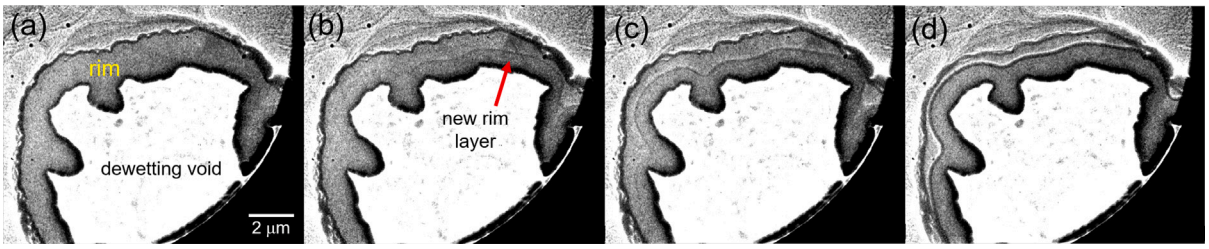

Fig. 5. Sequence of LEEM images showing the formation of a new rim layer, electron energy 0.8 eV, 1240 K. (a): a dewetting void that has not yet formed branched fingers is surrounded by a rim that displays a surface without steps, like the rim imaged by AFM in Fig. 2(a). (b): a new rim layer has nucleated on the right of the void and is growing around the void towards the left of the image. (c): the rim layer has completely surrounded the void, a step is visible on the rim surface. (d): the rim layer extends towards the exterior of the void.

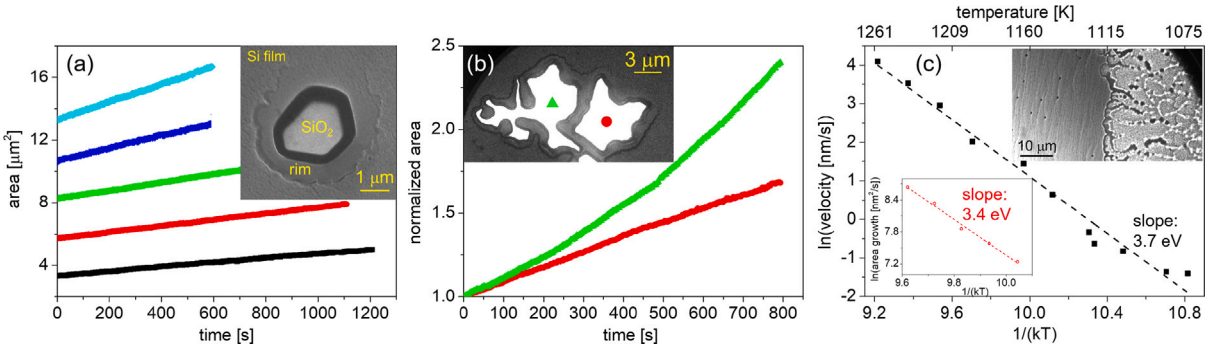

Fig. 6. (a): Area growth as a function of time of a dewetting void in the first stages, before the development of branched fingers. The void area grows linearly with time, with different slopes according to the temperature. From the bottom to the top, black: 1155 K, red: 1170 K, green: 1180 K, blue: 1195 K, light blue: 1205 K. (b): area growth as a function of time of two voids at 1125 K. The void that develops branched fingers (green triangles) grows non-linearly with time and faster than the other void (red circles). The inset shows the two voids at the end of the measurements. (c): natural logarithm of the velocity of a fingered dewetting front as a function of 1/(kT). The dashed line is a linear fit through the data points. The inset shows the fingered front used for the velocity measurements. (For interpretation of the references to color in this figure legend, the reader is referred to the web version of this article.)

This observation proves a layer-by-layer growth mode of the rim for SOI(111), as also observed in dewetting of SOI(100).

4. Kinetics

We have studied by LEEM the kinetics of void opening as a function of time and temperature. Fig. 6a shows the area growth of the same void as a function of time for different temperatures. As shown in the inset of Fig. 6a, the void is approximately hexagonal and has not yet developed fingers. In these early stages the void area increases linearly with time. Pierre-Louis et al. have shown theoretically and with simulations that the area of dewetting voids increases linearly with time when the rim height increases via the nucleation of new layers [31], which is what we observe (see Fig. 5). As expected, for higher temperatures the void area grows faster. Writing the area growth as a thermally activated process, $\frac{dA}{dt} = C\exp(-E_{eff}/(kT))$, it is possible to extract an effective activation energy E_{eff} by plotting the natural logarithm of the dewetting area growth as a function of 1/(kT), shown in the inset of Fig. 6c. From the slope of the linear fit through the data points, we find $E_{eff} = 3.4\pm0.2$ eV. Fig. 6b shows the area change of two voids, one of which is developing fingers. A LEEM image of the voids at the end of the measurements is shown in the inset of Fig. 6b. The right void (red circle) keeps approximately straight edges and only towards the end of the measurements the corners of the hexagon destabilize. The area of this void grows linearly with time. The area of the left void, marked with a green triangle, grows faster as void fingers form. The formation of fingers clearly leads to an increase of the area growth versus time. With the formation of fingers, the dewetting mechanism changes, nucleation of new rim layers is no more necessary, as atoms leave the tip of fingers and are incorporated in the steps of the rim of the finger edges. Large dewetted areas with edges formed by many advancing fingers display dewetting fronts that advance linearly with time. The velocity of these fronts increases with the temperature. With an analysis similar to that done for the measurements of the void area growth, we can obtain another effective energy $E'_{eff} = 3.7\pm0.2$ eV [32]. Considering that the SOI(111) samples are 30 nm thick, and that the effective dewetting energy increases with the film thickness, this value is consistent with that found from the front velocities in SOI(100) (3.4 ± 0.2 for 22 nm thick SOI(100), [14]). Notice that Cheynis et al. [14], have shown that the effective energy involved in the dewetting front velocity is not only related to the energies of diffusion and adatom creation (E_{diff} and E_c), but also involves the height h and the width w of the rim at the finger tip, which in turn depend on the temperature ($v_{front} \propto \frac{\exp(-(E_{diff}+E_c)/(kT))}{kT\cdot h^2 w}$).

5. Kinetic Monte Carlo model

Figs. 7(a)–(d) show a sequence of images extracted from the KMC simulation of the shape of a void growing by dewetting in a film consisting of three layers. In the early stages the void is hexagonal and the surrounding rim has uniform height growing layer by layer. In later stages the development of fingers and the formation of a total dewetted area with triangular shape is similar to the experimentally observed shapes (see Figs. 1d and 4c). The dewetting voids keep longer time a hexagonal shape in simulations performed at low temperatures. Fingers preferentially propagate in the [1-21], [11-2] and [-211] directions.

Fig. 8 shows some snapshots of the simulation of the growth of a void in a vicinal terrace. The following discussion is based on the color version of the figure. Comparing Figs. 8a and 8b, we observe that atoms removed from the void edges diffuse on the film and attach to nearby steps. Therefore both steps close to the void (the one on the right and that on the left) move in the step-down direction, i.e. towards the left. When the higher terrace reaches the void, it forms a rim around the void as shown in Fig. 8c. The rim is actually the extension of the upper

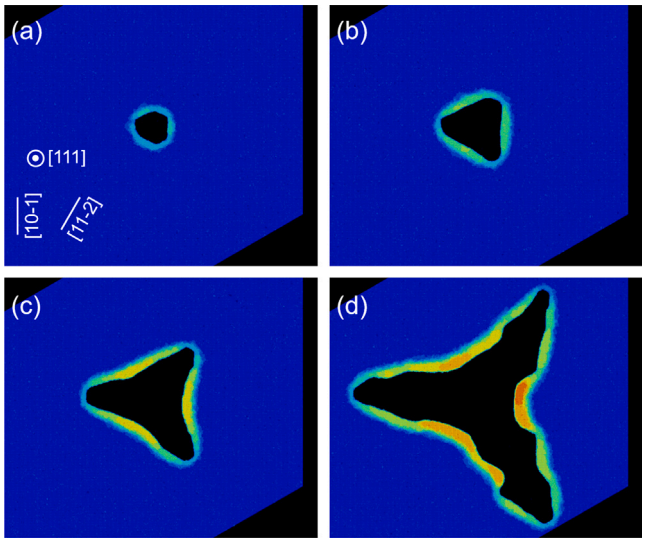

Fig. 7. Sequence of images of a KMC simulation of a fcc dewetting thin film of 3 layers, $kT = 0.65$ J. The starting film surface is not vicinal but a perfectly flat (111) terrace. After the formation of a hexagonal void in the first stages of dewetting (time from start: $0.6 \cdot 10^7 \nu_0^{-1}$), void fingers develop perpendicularly to the short edges of the hexagon (time: $2.0 \cdot 10^7, 4.0 \cdot 10^7$ and $7.6 \cdot 10^7 \nu_0^{-1}$ for (b), (c) and (d) respectively). The dewetting morphology is comparable to the experimental one (see Fig. 4c).

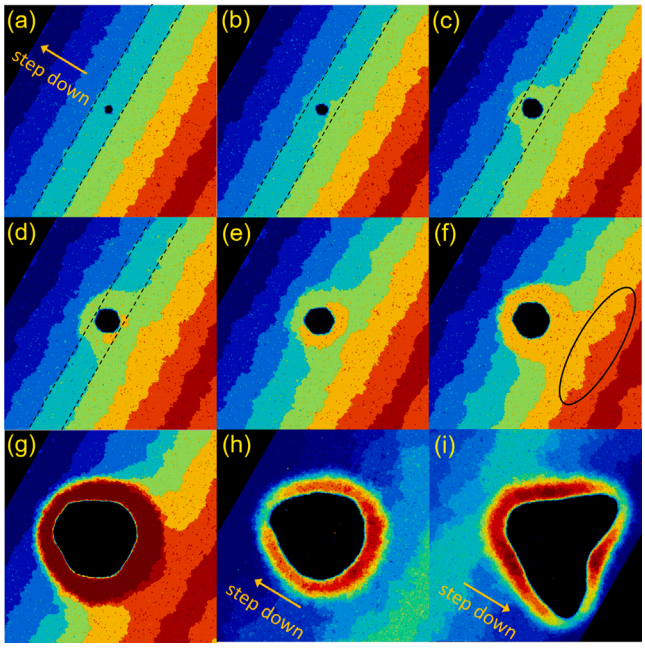

Fig. 8. Sequence of images of a KMC simulation of a dewetting void growing on a vicinal surface. In a-g, $kT = 0.65$ J and the surface terraces have increasing height from dark blue (top-left, 4 layers) to dark red (bottom-right, 11 layers). The steps run along the [10-1] direction. The step-down direction is the [1-21]. The dashed lines show the positions of the steps close to the void at the beginning of the simulation (a): The void grows at first without rim formation, as the film atoms removed from the void edges are captured by the nearby surface steps; time: $0.6 \cdot 10^6 \nu_0^{-1}$. (b–c): The upper terrace adjacent to the void grows and surrounds the dewetting void; time: $2.4 \cdot 10^6$ and $9.4 \cdot 10^6 \nu_0^{-1}$. (d–e): atoms removed from the bottom right side of the void are no more captured by the upper terrace step (yellow), that is too far, but they meet and form nuclei of a new rim layer that grows; time: $13.6 \cdot 10^6$ and $15.3 \cdot 10^6 \nu_0^{-1}$ (f): the rim grows all around the void and also joins the upper yellow terrace, time: $17.1 \cdot 10^6 \nu_0^{-1}$. The black ellipse shows Bales–Zangwill instabilities [33] of the upper step that receives the adatom flux from the dewetting void. (g): in later stages (time $1.4 \cdot 10^8 \nu_0^{-1}$) the rim around the void does not reach the upper terrace. (h): the step train is the same as in (a)–(g), the temperature is higher, $kT = 0.85$ J, and the terrace color code is adjusted (dark red corresponds to a height of 17 layers); time: $2.6 \cdot 10^7 \nu_0^{-1}$. (i): same as h but the step down direction is towards the bottom right, [-12-1]; time: $3.6 \cdot 10^7 \nu_0^{-1}$. (For interpretation of the references to color in this figure legend, the reader is referred to the web version of this article.)

terrace and is therefore wider on the side of the upper terraces (right in Fig. 8a). Far from the void, the step positions are roughly unchanged (but, since there is an atomic flux coming from the dewetting void, the steps can present morphological instabilities of the Bales–Zangwill kind [33], see the black ellipse in Fig. 8f). The next rim layer is formed in the same way, unless the distance between the next upper terrace and the void edge is large: In this case the next rim layer is formed by nucleation, when some atoms meet, as shown in Fig. 8d. One or more nuclei of the new layer form on the side of the upper terraces, because in the step-down direction the rim is narrow and atoms diffusing in this direction are easily incorporated in the nearby steps (in our KMC model there is no Schwoebel barrier [34]). The atoms detaching from the edges of the growing void make the new rim layer extend around the void (Fig. 8e). Further growth of the void makes the rim expand towards the upper terrace, until the rim and the upper terrace meet (Fig. 8f). The process continues with the sequence described above, but in later stages the rim grows in height without reaching the upper terrace, as shown in Fig. 8g. Notice that the rim on this side is wider, therefore the void shape will more likely destabilize and form fingers in the step-down direction, i.e. on the lower-terrace side, where the rim is narrow. Increasing the temperature to accelerate dewetting, we have observed the destabilization of the hexagonal void and the formation of fingers in the step-down direction, as shown in Fig. 8h. In simulations performed with the step down direction corresponding to the [-12-1], that does not correspond to an easy direction of propagation of fingers, the destabilization of the void occurs with formation of fingers that propagate towards lower terraces, but in the [-211] and [11-2] directions (see Fig. 8i).

6. Summary

In this work we have shown that the step-train orientation of a vicinal surface significantly affects solid state dewetting. We have studied the dewetting of SOI close to the (111) orientation, using different experimental techniques. Hexagonal voids grow in the Si film by developing an asymmetric rim, which is wider on the higher-terrace side than on the lower-terrace one. We have demonstrated the growth of the rim layer by layer around dewetting voids in the early dewetting stages, i.e. before the development of branched fingers. Dewetting fingers develop faster and are thinner in the step-down than in the step-up direction. KMC simulations allow us to understand the mechanisms of rim and finger formation that we observe experimentally. In the early dewetting stages, nucleation of a new rim layer is not necessary: atoms leaving the dewetting void are captured by the closer upper step, therefore the upper terrace grows and surrounds the dewetting void. Nucleation of a new rim layer is only necessary when the distance between the edge of the void and the upper terrace is very large. Finally, the dewetting kinetics in SOI(111) is consistent with the modeling and the energies previously reported for SOI(100).

CRediT authorship contribution statement

Stefano Curiotto: Conceptualization, Investigation, Data curation, Formal analysis, Funding acquisitions, Software, Writing – original draft, Writing – review & editing. **Pierre Müller:** Funding acquisitions, Writing – review & editing, Validation. **Fabien Cheynis:** Writing – review & editing, Validation. **Igor Ozerov:** investigation, Writing – review & editing, Validation. **Frédéric Leroy:** Conceptualization, Writing – review & editing, Validation.

Declaration of competing interest

The authors declare the following financial interests/personal relationships which may be considered as potential competing interests: Stefano Curiotto reports financial support was provided by French National Research Agency. If there are other authors, they declare that they have no known competing financial interests or personal relationships that could have appeared to influence the work reported in this paper.

Data availability

Data will be made available on request.

Acknowledgments

This work has been supported by the ANR grant Thermotweez, France (ANR-22-CE09-0009-01). We thank A. El-Bouich for sample preparation and A. Ranguis for the AFM measurements. We acknowledge the nanofabrication platform PLANETE (CT PACA, RENATECH+) for technical support.

Appendix A. Supplementary data

Movie 1 shows a LEEM image sequence of a dewetting void where nucleation and growth of a new atomic layer on top of the rim is clearly observed. The image width is 12.5 μm, the duration is 179 s, MEM to LEEM observation mode with electron energy 0.8 eV.

Supplementary material related to this article can be found online at https://doi.org/10.1016/j.surfin.2024.103912.

References

[1] S.-L. Zhang, M. Ostling, Metal silicides in CMOS technology: Past, present, and future trends, Crit. Rev. Solid State Mater. Sci. 28 (2003) 1.
[2] B. Legrand, V. Agache, J.P. Nys, V. Senez, D. Stievenant, Formation of silicon islands on a silicon on insulator substrate upon thermal annealing, Appl. Phys. Lett. 76 (2000) 3271.
[3] F. Leroy, L. Borowik, F. Cheynis, Y. Almadori, S. Curiotto, M. Trautmann, J. Barbé, P. Müller, How to control solid state dewetting: A short review, Surf. Sci. Rep. 71 (2016) 391–409.
[4] Y. Ishikawa, M. Kumezawa, R. Nuryadi, M. Tabe, Effect of patterning on thermal agglomeration of ultrathin silicon-on-insulator layer, Appl. Surf. Sci. 190 (2002) 11.
[5] Y. Ishikawa, Y. Imai, H. Ikeda, M. Tabe, Pattern-induced alignment of silicon islands on buried oxide layer of silicon-on-insulator structure, Appl. Phys. Lett. 83 (2003) 3162.
[6] A.L. Giermann, C.V. Thompson, Three-dimensional graphoepitaxial alignment resulting from solid-state dewetting of Au films on surfaces with monoperiodic topography, Appl. Phys. Lett. 101 (2012).
[7] M. Naffouti, T. David, A. Benkouider, L. Favre, A. Delobbe, A. Ronda, I. Berbezier, M. Abbarchi, Templated solid-state dewetting of thin silicon films, Small 12 (2016) 1–8.
[8] J. Ye, C.V. Thompson, Templated solid-state dewetting to controllably produce complex patterns, Adv. Mater. 23 (2011) 1567–1571.
[9] M. Abbarchi, M. Naffouti, B. Vial, A. Benkouider, L. Lermusiaux, L. Favre, A. Ronda, S. Bidault, I. Berbezier, N. Bonod, Wafer scale formation of monocrystalline silicon-based Mie resonators via silicon-on-insulator dewetting, ACS Nano 8 (2014) 11181–11190.
[10] M. Trautmann, F. Cheynis, F. Leroy, S. Curiotto, O. Pierre-Louis, P. Müller, Dewetting of patterned solid films: Towards a predictive modelling approach, Appl. Phys. Lett. 110 (2017) 263105.
[11] M. Trautmann, F. Cheynis, F. Leroy, S. Curiotto, P. Müller, Interplay between deoxidation and dewetting for ultrathin SOI films, Appl. Phys. Lett. 110 (2017) 161601.
[12] D.T. Danielson, D.K. Sparacin, J. Michel, L.C. Kimerling, Surface-energy-driven dewetting theory of silicon-on-insulator agglomeration, J. Appl. Phys. 100 (2006) 083507.
[13] F. Leroy, F. Cheynis, T. Passanante, P. Müller, Dynamics, anisotropy, and stability of silicon-on-insulator dewetting fronts, Phys. Rev. B 85 (2012).
[14] F. Cheynis, E. Bussmann, F. Leroy, T. Passanante, P. Müller, Dewetting dynamics of silicon-on-insulator thin films, Phys. Rev. B 84 (2011).
[15] F. Cheynis, F. Leroy, T. Passanante, P. Müller, Agglomeration dynamics of germanium islands on a silicon oxide substrate: A grazing incidence small-angle X-ray scattering study, Appl. Phys. Lett. 102 (2013) 161603.
[16] F. Cheynis, F. Leroy, P. Müller, Dynamics and instability of solid state dewetting, C. R. de Phys. 14 (2013).
[17] S. Curiotto, F. Leroy, F. Cheynis, P. Müller, Oxygen-induced inhibition of silicon-on-insulator dewetting, Appl. Phys. Lett. 104 (2014) 061603.
[18] H. Nahor, H. Meltzman, W.D. Kaplan, Ni-YSZ(111) solid-solid interfacial energy, J. Mater. Sci. 49 (2014) 3943.
[19] G. Katz, The epitaxy of copper on sapphire, Appl. Phys. Lett. 12 (1968) 161.
[20] K.E. Harris, V.V. Singh, A.H. King, Grain rotation in thin films of gold, Acta Mater. 46 (1998) 2623.
[21] E. Bussmann, F. Cheynis, F. Leroy, P. Müller, Thermal instability of silicon-on-insulator thin films measured by low-enregy electron microscopy, in: IOP Conference Series: Materials Science and Engineering, vol. 12, 2010, p. 1.
[22] E. Bauer, LEEM basics, Surf. Rev. Lett. 5 (1998) 1275–1286.
[23] S. Ino, Some new techniques in reflection high energy electron diffraction (RHEED) application to surface structure studies, Japan. J. Appl. Phys. 16 (1977) 891–908.
[24] A.F. Voter, Radiation Effects in Solids, Springer, NATO Publishing Unit, Dordrecht, The Netherlands, 2005.
[25] S. Curiotto, A. Chame, P. Müller, C.V. Thompson, O. Pierre-Louis, Hole opening from growing interfacial voids: A possible mechanism of solid state dewetting, Appl. Phys. Lett. 120 (2022) 091603.
[26] K. Sudoh, M. Naito, Interfacial reaction of Si islands on SiO2 during high-temperature annealing, J. Appl. Phys. 108 (2010) 083520.
[27] F. Leroy, Y. Saito, S. Curiotto, F. Cheynis, O. Pierre-louis, P. Müller, Shape transition in nano-pits after solid-phase etching of SiO2 by Si islands, Appl. Phys. Lett. 106 (2015) 191601.
[28] Y. Ono, M. Nagase, M. Tabe, Y. Takahashi, Thermal agglomeration of thin single crystal Si on SiO2 in vacuum, Japan. J. Appl. Phys. 34 (1995) 1728.
[29] Z.A. Burhanudin, R. Nuryadi, Y. Ishikawa, M. Tabe, Y. Ono, Thermally-induced formation of Si wire array on an ultrathin (111) silicon-on-insulator substrate, Appl. Phys. Lett. 87 (2005) 121905.
[30] E. Shaffir, I. Riess, W. Kaplan, The mechanism of initial de-wetting and detachment of thin Au films on YSZ, Acta Mater. 57 (2009) 248–256.
[31] O. Pierre-Louis, A. Chame, Y. Saito, Dewetting of ultrathin solid films, Phys. Rev. Lett. 103 (2009) 195501.
[32] Dewetting is at the origin of both, hole-area growth and dewetting front propagation, however the processes are different and thus the effective energies do not have to correspond ($E_{eff} \neq E'_{eff}$).
[33] G.S. Bales, A. Zangwill, Morphological instability of a terrace edge during step-flow growth, Phys. Rev. B 41 (1990) 5500.
[34] R.e. Schwoebel, E.J. Shipsey, Step motion on crystal surfaces, J. Appl. Phys. 37 (1966) 3682.